Fractional delay filter based repetitive control for precision tracking: Design and application to a piezoelectric nanopositioning stage

Zhao Feng [a,b], Min Ming [b], Jie Ling [c,*], Xiaohui Xiao [b], Zhi-Xin Yang [d], Feng Wan [a,e,*]

[a] Department of Electrical and Computer Engineering, University of Macau, Macao, China
[b] School of Power and Mechanical Engineering, Wuhan University, Wuhan, 430072, China
[c] College of Mechanical & Electrical Engineering, Nanjing University of Aeronautics and Astronautics, Nanjing, 210016, China
[d] State Key Laboratory of Internet of Things for Smart City and Department of Electromechanical Engineering, University of Macau, Macao, China
[e] Centre for Artificial Intelligence and Robotics, Institute of Collaborative Innovation, University of Macau, Macao, China

ARTICLE INFO

ABSTRACT

The development of nanotechnology requires a precision tracking of periodic signals in order to complete repetitive industrial or scientific tasks. Although repetitive control is an intuitive choice to realize precisely periodic signal's tracking, an integer number should match the period of signals for a digital control system otherwise the performance would be deteriorated significantly. Thus, in this paper, a fractional delay filter based repetitive control (FDFRC) is developed to achieve precision signal tracking with arbitrary periods. According to the internal model principle, a fractional delay filter with the spectrum-selection property is designed by using of a Farrow structure to address integer/non-integer delays. The stability of FDFRC is also given and analyzed in frequency domain to facilitate controller implementation. The proposed FDFRC allows an easy, simple and practical realization with only one parameter to be adjusted for different integer/non-integer delays. Comparative experiments with different frequencies of triangular waves for x axis and Lissajous scanning for x–y plane on a piezoelectric nanopositioning stage are conducted to further verify the significant improvements on the tracking performance of the proposed controller.

1. Introduction

The rapid development of nanotechnology requires a precision trajectory tracking of the devices for various tasks [1]. For the applications in micro/nano scale, the piezoelectric nanopositioning stage is a widely used device to obtain nanometer or subnanometer precision [2]. Through integrating with flexure-based compliant mechanisms, a transmit motion is generated without friction and backlash [3]. The piezoelectric nanopositioning stages have been widely employed in micromanipulation systems [4], fast tool servo systems [5], and scanning probe microscopes [6]. More specifically, the image quality of the sample for scanning probe microscopes are largely determined by the tracking precision of the piezoelectric nanopositioning stages. However, the indigenous hysteresis of piezoelectric actuators and resonance caused by the light damping property deteriorate the tracking performance significantly.

Nomenclature

α, β	Parameters of zero-phase filter
$C(z^{-1})$	Baseline feedback controller
d	Compensation delay term in RC
f_r	Frequency of $r(k)$
f_s	Sampling rate
K	Order of the fractional delay filter
k	Sampling point
$L(z^{-1})$	Learning filter
N	Number of samples in one period of a periodic signal
N^*	Integer part of N
p	Non-integer part of N
$P(z^{-1})$	Discrete linear system
$r(k)$	Periodic reference
$u(k)$	Control input
$y(k)$	Plant output
z^{-1}	Unit delay operator
FBC	Baseline feedback controller
FDFRC	Fractional delay filter based repetitive control
FORC	Fractional-order repetitive controller
RC	Repetitive control
TRC	Traditional repetitive controller

The hysteresis nonlinearities of piezoelectric nanopositioning stages can be removed through modeling and feedforward compensation by using different hysteresis models (see [7,8]). However, the methods need a time-consuming modeling process to describe an accurate hysteresis model. Alternatively, robust control schemes such as sliding mode control are effective to eliminate hysteresis and improve tracking precision without complex modeling [9]. Furthermore, in order to reduce the motion vibrations, some damping controllers also have been designed to increase the damping coefficient of the piezo-actuated stages [10]. It is worth noting that the previous mentioned control schemes are generally designed based on a second-order plant.

As a consequence, repetitive control (RC) is suitable to track such motion process with large performance improvement. According to the internal model principle [11], the infinite gains at the fundamental frequency as well as the harmonics of the reference or disturbance are generated so that a zero steady-state error is achieved [12]. As a learning-based controller in time domain, RC can be implemented without resetting to the initial states in comparison with iterative learning control that works in iteration domain [13,14]. Various RC methods have been proposed, such as RC with different stability criteria [15,16], and predictive RC [17]. In [18,19], the robust RCs through integrating with equivalent input disturbance observer were proposed and designed in continuous-time domain. In view of the application of nanopositioning stages, the discrete-time RCs incorporating Prandtl–Ishlinskii compensation model were developed and analyzed to address the hysteresis nonlinearity [20,21]. Note that the above methods require the accurate hysteresis compensation. Based on the experimental results, the hysteresis nonlinearity caused errors are always at the harmonics of the input periodic reference so that the odd-harmonic RC was utilized to circumvent hysteresis modeling [22].

In general, the discrete-time repetitive control is realized by inserting the term $1/(1 - z^{-N})$, where N is the number of sample points per period of the signal of a digital control system. For the previous mentioned RC design, it is always satisfied that N is an integer. Nevertheless, this condition is rigorous for some applications thus the tracking frequency cannot be chosen arbitrarily, especially for a low sampling rate. For example, the ratio of x and y frequencies for Lissajous scanning should be assigned as a rational number [23]. If the nearest integer of N is used in RC, the tracking performance is deteriorated significantly. To address this problem, multirate RC is proposed so that RC is implemented with a variable sampling rate to make N an integer [24,25]. However, the implementation of varied control structure is complex and may result in destabilization.

For systems with fixed sampling rate, the mentioned issue will lead to the fractional order controller. In [26], a set of tuning rules for integer-order PID and fractional-order PID controllers were developed. Also in [27], a novel auto-tuning method to ensure the robustness for fractional order PI/PD controllers was proposed. A low-order, computationally stable and efficient method for direct approximation of general fractional order controllers in the form of discrete-time rational transfer functions was developed in [28], and the development of fractional-order hysteresis model was built in [29]. More details about fractional order control focusing on feedback control and stability can be found in [30,31]. In concern with the RC with fractional delay on practical applications, the Lagrange interpolating to approximate the fractional delay is a widely used method for a fixed sampling rate system. For example, the fractional repetitive control with a fractional lead filter was designed for pulse width modulation inverter based on Lagrange interpolation [32].
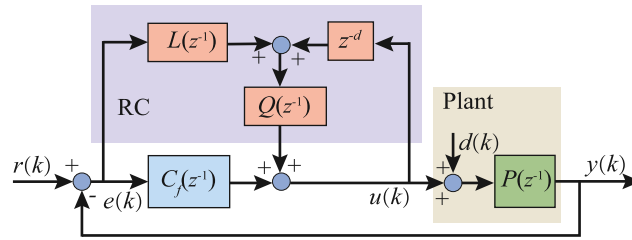
Fig. 1. Block diagram of RC scheme with a series–parallel implementation based on the spectrum-selection filter.

In order to compensate hysteresis and improve tracking accuracy, a plugged-in fractional repetitive control for nanopositioning stages was proposed in [33]. However, it should be noted that the non-integer delay coefficients approximated by the Lagrange interpolation are changed with the non-integer delay parameter so that the fractional filter should be redesigned for signals with different frequencies. Furthermore, to enhance the flexibility when implementing RC, a spectrum-selection filter was integrated in RC to balance the convergence speed and robustness to external disturbances [34,35]. However, the delay number N should be an integer when implementing the above controllers.

Motivated by aforementioned essential issues, the fractional delay filter based repetitive control (FDFRC) for precision tracking is proposed to provide a comprehensive solution to the non-integer delay in the fixed sampling rate system and a significant performance improvement for the piezoelectric nanopositioning stage. The main contributions of this paper are listed below.

- A spectrum-selection based fractional delay filter is proposed, analyzed and implemented in Farrow structure to address the integer/non-integer delays so that the infinite gains at the harmonics of the periodic signal are obtained.
- The stability of FDFRC is analyzed and given in frequency domain based on the approximated filter for practical implementation.
- Various experiments on a piezoelectric nanopositioning stage are conducted to test the controller's performance under periodic signals input of different frequencies through comparisons.

The method in this paper to construct the fractional delay is realized by a Farrow structure so that the fractional delay filter can be deployed without redesigning the relevant coefficients for different integer/non-integer delays. Thus, the proposed FDFRC is easy to implement for systems subjecting to various periodic references with different frequencies in comparison with the methods in [20,21,33].

This paper begins with an overview of RC and the problem of fractional delay in Section 2. The detailed design and analysis of FDFRC as well as its stability in frequency domain are given in Section 3. The experimental setup and performance analysis of a piezoelectric nanopositioning stage are shown in Section 4. Experimental results of different reference signals are elaborated and discussed in Section 5, and Section 6 gives the conclusion.

2. Preliminaries and problem formulation

RC is an effective method to track periodic references or compensate periodic disturbances. For the general RC [21] or odd-harmonic RC [22], the main drawback is that the errors or disturbances can be amplified if the frequency spectrum is located at the non-harmonics of the fundamental frequency due to the waterbed effect. In [34], the RC scheme using spectrum-selection filter was proposed to make a trade-off between the convergence speed and robustness.

The block diagram of RC scheme based on the spectrum-selection filter for the piezoelectric nanopositioning stage is given in Fig. 1. To avoid the complex hysteresis modeling, the plant is described as a discrete linear system $P(z^{-1})$ cascaded with a bounded disturbance $d(k)$. The tracking error is calculated by $e(k) = r(k) - y(k)$, and $Q(z^{-1})$ is the spectrum-selection filter to generate high gains on the fundamental frequency and its harmonics. Therefore, according to Fig. 1, the overall controller integrating with RC and $C_f(z^{-1})$ is expressed as

$$C(z^{-1}) = \frac{C_f(z^{-1}) + Q(z^{-1})L(z^{-1})}{1 - z^{-d}Q(z^{-1})}. \tag{1}$$

Based on (1), the sensitivity transfer function from $r(k)$ to $e(k)$ is derived as

$$S_{RC}(z^{-1}) = \frac{1 - z^{-d}Q(z^{-1})}{1 + P(z^{-1})C_f(z^{-1}) + Q(z^{-1})(L(z^{-1})P(z^{-1}) - z^{-d})}. \tag{2}$$

To generate notches at the fundamental frequency and its harmonics, and to eliminate the distortion in the passband, a spectrum-selection filter is designed as [34,35]

$$Q_c(z^{-1}) = \frac{(1 - \rho)z^{-(N-d)}}{1 - \rho z^{-N}}, \rho \in [0, 1). \tag{3}$$
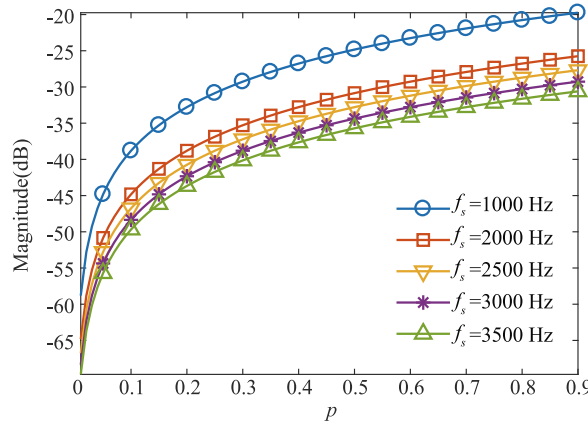
Fig. 2. Sensitivity of $|S_n(z^{-1})|$ for different p and f_s with $h = 1$, $\rho = 0.4$.

Substituting (3) into the numerator of (2), we can obtain that

$$S_n(z^{-1}) = 1 - z^{-d}Q_c(z^{-1}) = \frac{1 - z^{-N}}{1 - \rho z^{-N}}. \tag{4}$$

Therefore, $|S_{RC}(z)^{-1}|$ will be equal to zero if N is the exact number of sample points per period of the reference, which is an integer in general. It should be noted that with the increase of ρ, the convergence speed is decreased while the robustness to non-periodic errors is improved, and vice versa. Furthermore, in order to reduce the noise and model uncertainties, a low-pass filter is given as

$$Q_r(z^{-1}) = \alpha z^{-1} + \beta + \alpha z, \tag{5}$$

where the parameters should satisfy that $2\alpha + \beta = 1$, and the property of zero phase retains with the non-causal term αz. Although $Q_r(z^{-1})$ is a non-causal filter, its causal application can be ensured by the delay term $z^{-(N-d)}$ in $Q_c(z^{-1})$ so that it can be implemented in practical systems. Therefore, the spectrum-selection filter is designed as

$$Q(z^{-1}) = Q_c(z^{-1})Q_r(z^{-1}) = \frac{(1-\rho)(\alpha z^{-1} + \beta + \alpha z)z^{-(N-d)}}{1 - \rho z^{-N}}. \tag{6}$$

It should be noted that N in general is chosen as an integer, and calculated by f_s/f_r. However, the control scheme cannot track signals with arbitrary periods for a fixed f_s when N is a non-integer number. In this situation, assuming that $N = N^* + p$, where $N^* = int[N]$ is the integer part and $0 < p < 1$ is the fractional part. Moreover, $|S_n(z^{-1})|$ can be expressed as

$$\begin{aligned}
|S_n(z^{-1})| &= \frac{|1 - e^{-j\omega N/f_s}|}{|1 - \rho e^{-j\omega N/f_s}|} = \sqrt{\frac{1 - \cos(2\pi h f_r N/f_s)}{1 - \rho \cos(2\pi h f_r N/f_s)}} \\
&= \sqrt{\frac{1 - \cos(2\pi h f_r(N^* + p)/f_s)}{1 - \rho \cos(2\pi h f_r(N^* + p)/f_s)}},
\end{aligned} \tag{7}$$

where $\omega = 2\pi h f_r$ with h being the harmonic order.

To demonstrate the influence of fractional delay p and sampling rate f_s on the tracking performance, the amplitudes of $S_n(z^{-1})$ are plotted in Fig. 2. With p varying from 0 to 0.9, the gains of $S_n(z^{-1})$ are increased so that the tracking performance is significantly degraded according to (2). Furthermore, for a fixed p, the error can be alleviated by increasing f_s at the cost of computing burden. Therefore, the fractional delay poses a great challenge for RC to track references with non-integer delays in a digital control system.

3. Fractional delay filter based repetitive control

3.1. Design of fractional delay filter $Q(z^{-1})$

In this section, a fractional delay filter with spectrum-selection property is designed, and the fractional delay is constructed by a Farrow structure so that the fractional delay filter can be realized without redesigned the fractional delay coefficients for different integer/non-integer delays. The non-integer delay N can be decomposed as

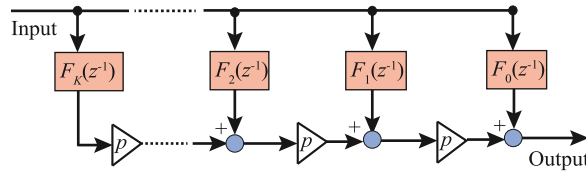$$z^{-N} = z^{-(N^*+p)} = z^{-N^*} \cdot z^{-p}, \tag{8}$$

Fig. 3. The implementation of $G_f(z, p)$ using the Farrow structure.

where z^{-p} is the fractional delay. Based on the Taylor Series expansion to a polynomial in p, z^{-p} can be rewritten as

$$
\begin{aligned}
z^{-p} &= e^{-j\omega p} = \sum_{k=0}^{\infty} \frac{(-j\omega)^k}{k!} (p)^k \\
&= \sum_{k=0}^{K} \frac{(-j\omega)^k}{k!} (p)^k + O(p^{K+1}),
\end{aligned}
\tag{9}
$$

where $O(p^{K+1})$ denotes a higher-order term which is approximated to zero, and K is the order of the polynomial. Thus, it is obtained that

$$
e^{-j\omega p} \approx \sum_{k=0}^{K} \frac{(-j\omega)^k}{k!} p^k = \sum_{k=0}^{K} F_k(z^{-1}) p^k,
\tag{10}
$$

where $F_0(z^{-1}), F_1(z^{-1}), F_2(z^{-1}), \ldots, F_K(z^{-1})$ are the sub-filter to be determined, and the implementation can be realized through the Farrow structure shown in Fig. 3. Furthermore, the above equation is rewritten as

$$
G_f(z^{-1}, p) = \sum_{k=0}^{K} F_k(z^{-1}) p^k = \mathbf{p}^T \mathbf{F}(z^{-1}),
\tag{11}
$$

where

$$
\mathbf{p} = \begin{bmatrix} 1 \\ p \\ p^2 \\ \vdots \\ p^K \end{bmatrix}, \mathbf{F}(z^{-1}) = \begin{bmatrix} F_0(z^{-1}) \\ F_1(z^{-1}) \\ F_2(z^{-1}) \\ \vdots \\ F_K(z^{-1}) \end{bmatrix}.
\tag{12}
$$

Through implementing Lagrange interpolation, we can obtain that

$$
\begin{cases}
G_f(z^{-1}, 0) = F_0(z^{-1})0^0 + F_1(z^{-1})0^1 + .. + F_K(z^{-1})0^K = z^0, \\
G_f(z^{-1}, 1) = F_0(z^{-1})1^0 + F_1(z^{-1})1^1 + .. + F_K(z^{-1})1^K = z^{-1}, \\
\quad \vdots \\
G_f(z^{-1}, K) = F_0(z^{-1})M^0 + F_1(z^{-1})M^1 + .. + F_K(z^{-1})K^K = z^{-K},
\end{cases}
\tag{13}
$$

which is simplified as

$$
\mathbf{V}\mathbf{F}(z^{-1}) = \mathbf{z},
\tag{14}
$$

where

$$
\mathbf{V} = \begin{bmatrix} 0^0 & 0^1 & 0^2 & \cdots & 0^K \\ 1^0 & 1^1 & 1^2 & \cdots & 1^K \\ 2^0 & 2^1 & 2^2 & \cdots & 2^K \\ \vdots & \vdots & \vdots & \ddots & \vdots \\ K^0 & K^1 & K^2 & \cdots & K^K \end{bmatrix}, \mathbf{z} = \begin{bmatrix} z^0 \\ z^{-1} \\ z^{-2} \\ \vdots \\ z^{-K} \end{bmatrix}.
\tag{15}
$$

It is clear that $\mathbf{V}$ is a Vandermonde matrix. Therefore, the sub-filters $\mathbf{F}(z^{-1})$ can be rewritten as

$$
\mathbf{F}(z^{-1}) = \mathbf{V}^{-1}\mathbf{z},
\tag{16}
$$

and the fractional delay filter is given by

$$
G_f(z^{-1}, p) = \mathbf{p}^T \mathbf{V}^{-1}\mathbf{z}.
\tag{17}
$$

In order to test the performance of sub-filters for different orders K, the magnitude responses of $G_f(z^{-1}, p)$ are plotted in Fig. 4. For $K = 1$, the passband determined by ± 3 dB is the lowest at about 690 Hz, and for $K = 3, 5, 7$, the bandwidth are at about 760 Hz, 605 Hz, and 560 Hz, respectively. Therefore, $K = 3$ is selected in this paper to guarantee the best performance. In addition,
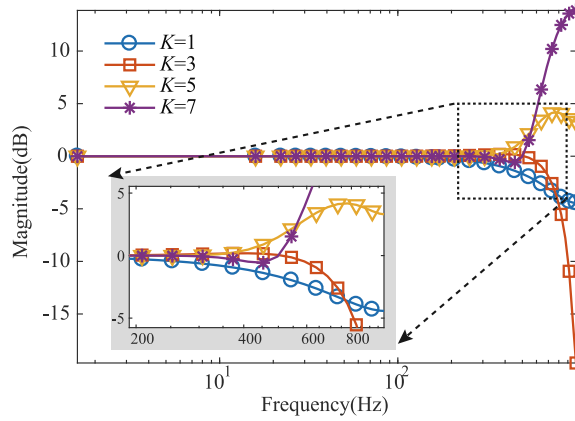
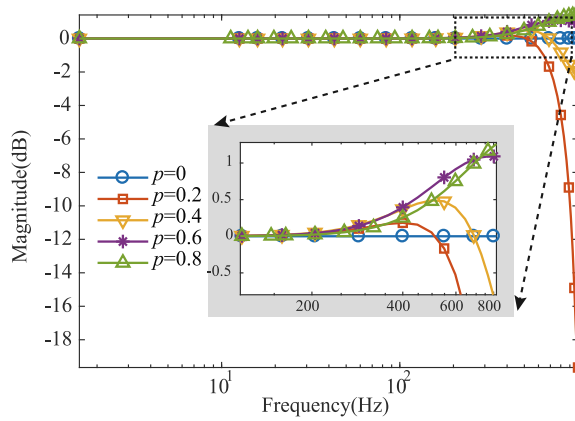**Fig. 4.** The magnitude responses of $G_f(z^{-1}, p)$ for different K with $p = 0.2, f_s = 2000$ Hz.

Fig. 5. The magnitude responses of $G_f(z^{-1}, p)$ for different p with $K = 3, f_s = 2000$ Hz.
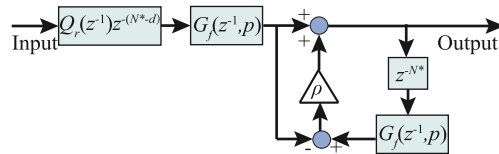

Fig. 6. The implementation of $Q(z^{-1})$ with fractional delay filter.

Fig. 5 gives the magnitude responses of $G_f(z^{-1}, p)$ to approximate different fractional delays p. It is obvious the filter is capable of fractional delay estimation in the low frequency band up to nearly 600 Hz, i.e., more than 60% of the Nyquist bandwidth.

Based on the fractional delay filter with the Farrow structure, the spectrum-selection filter with fractional delay in this paper is designed as

$$Q_{fc}(z^{-1}) = \frac{(1-\rho)z^{-(N^*-d)}G_f(z, p)}{1 - \rho z^{-N^*}G_f(z, p)}, \rho \in [0, 1), \tag{18}$$

Then, combining with the zero-phase low-pass filter $Q_r(z^{-1})$, the proposed fractional delay filter is designed as

$$Q(z^{-1}) = \frac{(1-\rho)(\alpha z^{-1} + \beta + \alpha z)z^{-(N^*-d)}G_f(z^{-1}, p)}{1 - \rho z^{-N^*}G_f(z^{-1}, p)}. \tag{19}$$

In order to realize (19) with a varied ρ to make a trade off between the convergence speed and robustness, the scheme of $Q(z^{-1})$ with fractional delay filter is proposed in Fig. 6 in this paper.

In addition, the performance of the fractional delay filter with spectrum-selection property is analyzed. With $f_s = 2000$ Hz and $f_r = 22$ Hz, the exact delay is calculated as $N = 90.909$ with a fractional delay $p = 0.909$. For $N = 90, 91, 90.909$, the magnitude
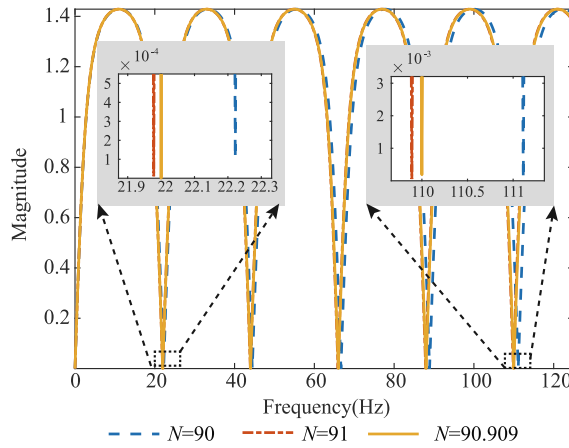
Fig. 7. The magnitude responses of $1 - Q(z^{-1})$ for different N with $\rho = 0.4, Q_r(z^{-1}) = 1, f_s = 2000$ Hz, $f_r = 22$ Hz.

responses of $1 - Q(z^{-1})$ are plotted in Fig. 7. At the fundamental frequency 22 Hz, the parameter with $N = 90$ is notched at 22.2 Hz, and that with $N = 91$ at 21.9 Hz, while the fractional delay filter makes the notch at 22 Hz exactly. For the 5th harmonic at 110 Hz, the proposed method also generates zero gain so that zero error is achieved. The above results demonstrate that the proposed fractional delay filter (19) can significantly address the non-integer delay for a fixed sampling rate.

3.2. Design of compensation filter $L(z^{-1})$

In generally, the compensation filter $L(z^{-1})$ is designed as the inversion of the linear plant $P(z^{-1})$. However, the nonminimum-phase zeros commonly exist for the flexure-based compliant devices [36]. Therefore, the model $P(z^{-1})$ is decomposed as

$$P(z^{-1}) = \frac{B_s(z^{-1})B_u(z^{-1})}{A(z^{-1})}, \tag{20}$$

where $B_s(z^{-1})$ contains the stable zeros, and the roots of $B_u(z^{-1})$ are outside the unit circle. $A(z^{-1})$ contains the stable poles. Furthermore, $B_u(z^{-1})$ can be rewritten as

$$B_u(z^{-1}) = b_n + b_{n-1}z^{-1} + b_{n-2}z^{-2} + \cdots + b_0 z^{-n}, \tag{21}$$

where n is the number of nonminimum-phase zeros. Through utilizing the zero-magnitude error tracking (ZMET) technology [37], $L(z^{-1})$ is designed as

$$L(z^{-1}) = \frac{A(z^{-1})}{B_s(z^{-1})B_u^f(z^{-1})} z^{-q}, \tag{22}$$

where $B_u^f(z^{-1})$ is given by

$$B_u^f(z) = b_0 + b_1 z^{-1} + b_2 z^{-2} + \cdots + b_n z^{-n}, \tag{23}$$

and q can be determined by the order of $A(z^{-1})$ minus the order of $B_s(z^{-1})B_u^f(z^{-1})$ to make $L(z^{-1})$ causal. Therefore, the delay term d is generally selected as $d \geq q$ taking into the sensor's delay in practice.

3.3. Stability analysis

In order to analyze the stability of the proposed method, the complementary sensitivity function from $r(k)$ to $y(k)$ according to Fig. 1 is deduced as

$$\begin{aligned} T_{RC}(z^{-1}) &= 1 - S_{RC}(z^{-1}) \\ &= \frac{P(z^{-1})C_f(z^{-1}) + L(z^{-1})P(z^{-1})Q(z^{-1})}{1 + P(z^{-1})C_f(z^{-1}) + Q(z^{-1})(L(z^{-1})P(z^{-1}) - z^{-d})}. \end{aligned} \tag{24}$$

Define that

$$Q_f(z^{-1}, p) = \frac{(1 - \rho)(\alpha z^{-1} + \beta + \alpha z)z^{-(N^* - d)}}{1 - \rho z^{-N^*} G_f(z^{-1}, p)}. \tag{25}$$

Substituting (25) into (24), it is obtained that

$$T_{RC}(z^{-1}) = \frac{P(z^{-1})C_f(z^{-1}) + L(z^{-1})P(z^{-1})Q_f(z^{-1})G_f(z^{-1})}{1 + P(z^{-1})C_f(z^{-1}) + Q_f(z^{-1}, p)G_f(z^{-1}, p)(L(z^{-1})P(z^{-1}) - z^{-d})}. \tag{26}$$

After rearrangement, the above equation is simplified as three transfer functions as

$$T_{RC}(z^{-1}) = H_1(z^{-1}) \frac{1}{1 + H_2(z^{-1})S_{FB}(z^{-1})}, \tag{27}$$

where

$$\begin{aligned} S_{FB}(z^{-1}) &= \frac{1}{1 + P(z^{-1})C(z^{-1})}, \\ H_1(z^{-1}) &= S_{FB}(z^{-1})[P(z^{-1})C_f(z^{-1}) + L(z^{-1})P(z^{-1})Q_f(z^{-1})G_f(z^{-1})], \\ H_2(z^{-1}) &= Q_f(z^{-1}, p)G_f(z^{-1}, p)(L(z^{-1})P(z^{-1}) - z^{-d}). \end{aligned} \tag{28}$$

Therefore, the stability of the closed-loop control system with FDFRC is guaranteed if the following conditions hold:

(1) The feedback controller $C_f(z^{-1})$ can stabilize the closed-loop system, i.e. $S_{FB}(z^{-1})$ is stable with all the roots of $1 + P(z^{-1})C_f(z^{-1})$ are inside the unit circle.
(2) The roots of $1 + H_2(z^{-1})S_{FB}(z)^{-1}$ should also be inside the unit circle, i.e.,

$$\left\| H_2(z^{-1})S_{FB}(z^{-1}) \right\| < 1. \tag{29}$$

With (28), we can further derive that

$$\left\| Q_f(z^{-1}, p)G_f(z^{-1}, p) \right\| < \left\| \frac{1 + P(z^{-1})C_f(z^{-1})}{L(z^{-1})P(z^{-1}) - z^{-d}} \right\|. \tag{30}$$

3.4. Design procedures

The design procedures of the proposed FDFRC are summarized as

(1) Determine the order K of the sub-filters $\mathbf{F}(z^{-1})$ to construct the Vandermonde matrix.
(2) Calculate the coefficients of the sub-filters using (16), and then get the fractional delay filter by (17).
(3) Design the fractional delay filter with spectrum-selection property with (19) and implement it by Figs. 3 and 6.
(4) Design the compensation filter (22) and check the stability using (30).

Remark 1. It should be noted that the bandwidth of the fractional delay approximated by the sub-filters is determined by f_s and K, and the bandwidth should be large enough to cover the frequency components of the periodic reference. For a digital system with a determined sampling rate, the larger order K may lead to a complex implementation and a smaller one will reduce the bandwidth. Thus, the choice of K with a fixed f_s is determined as 3 according to the magnitude responses in Fig. 4.

Remark 2. Note that once the order of the sub-filters K is determined, the coefficients of the sub-filters will be fixed. Therefore, the parameter p is the only variable in the Farrow structure shown in Fig. 3, which is easy to realize different fractional delays in comparison with traditional Lagrange interpolating method in [32,33], where the coefficients of the fractional delay should be redesigned for different signals.

Remark 3. The stability of the controller is given as (30) if $C(z^{-1})$ can stabilize $S_{FB}(z^{-1})$ through the discrete-time transfer functions. Although various methods to check the stability of the fractional order systems have been proposed [30,31,38], this paper concentrates on the overall stability when the fractional delay is approximated by $G_f(z^{-1}, p)$, i.e. the stability when implementing the controller. This is more practical and useful for guiding the actual experiments. The similar method is also used in [39–41].

Remark 4. Through the proposed FDFRC, the hysteresis caused errors located at the fundamental frequency and the harmonics can be compensated without complex and time-consuming modeling for periodic signals with non-integer N. This can be observed obviously from Fig. 7 in comparison with the design methods in [34,42].

4. Application to piezoelectric nanopositioning stages

4.1. Experimental setup

The proposed controller is verified on the nanopositioning stage with flexure-based compliant mechanism (model: P-561.3CD from Physik Instrumente). The control voltage is 0–10 V generated by PCI 6289 from National Instrument, and then sent to the piezo amplifier module E-503.00 to actuate the actuator. The measured position is got by the capacitive sensor and passed to the control
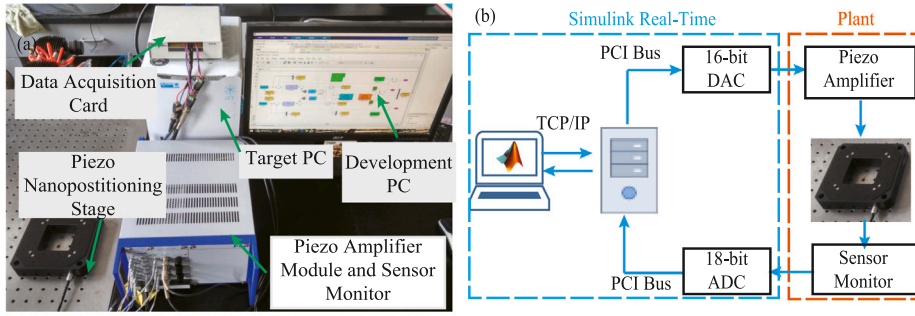
Fig. 8. The experimental setup of the piezoelectric nanopositioning stage. (a) experimental platform. (b) block diagram of control system.
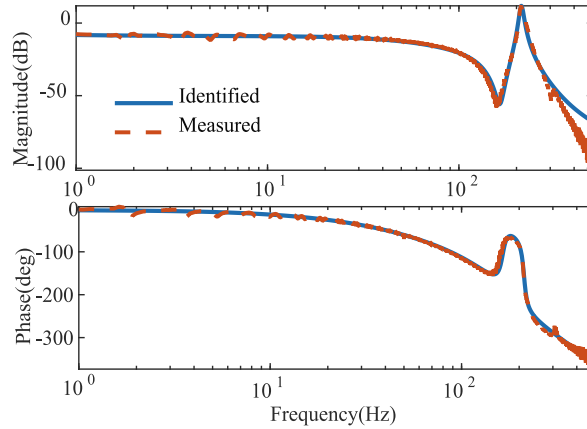

Fig. 9. Frequency responses of identified model and measured data for x axis.

system via data acquisition card PCI 6289. The control system is developed in MATLAB/Simulink software and built to the target PC to achieve real-time control. The detailed setup is illustrated in Fig. 8. The linear model used to design controller is identified as

$$P(z^{-1}) = \frac{0.012z^{-1} - 0.045z^{-2} + 0.109z^{-3} - 0.118z^{-4} + 0.532z^{-5}}{1 - 3.794z^{-1} + 6.25z^{-2} - 5.49z^{-3} + 2.556z^{-4} - 0.505z^{-5}}. \tag{31}$$

The frequency responses calculated by measured data and identified model (31) are given in Fig. 9, where it is obvious that $P(z^{-1})$ can describe the dynamics of the piezoelectric nanopositioning stage accurately enough. Furthermore, the first resonant frequency with a low damping ratio is located at 210 Hz, and a pair of nonminimum-phase zeros are at 165 Hz. Based on the model, we proceed to design the proposed FDFRC without modeling hysteresis nonlinearity. It should be noted that the dynamics of y axis is similar to that of x axis due to the symmetric structure. For simplicity, only the design and analysis for x axis are given in this section.

4.2. Controller implementation and performance analysis

The baseline feedback controller $C_f(z^{-1})$ is designed by combining a notch filter to reduce vibration and an integral term to enhance the steady-state tracking performance. After discretizing for digital system implementation, $C_f(z^{-1})$ is given as

$$C_f(z^{-1}) = \frac{0.063 - 0.037z^{-1} - 0.038z^{-2} + 0.061z^{-3}}{1 - 2.111z^{-1} + 1.963z^{-2} - 0.852z^{-3}}. \tag{32}$$

For the design of the sub-filters $\mathbf{F}(z^{-1})$, through using (15) and (16) selecting $K = 3$, we can obtain that

$$\begin{cases} F_0(z^{-1}) = 1, \\ F_1(z^{-1}) = -1.833 + 3z^{-1} - 1.5z^{-2} + 0.333z^{-3}, \\ F_2(z^{-1}) = 1 - 2.5z^{-1} + 2^{-2} - 0.5z^{-3}, \\ F_3(z^{-1}) = -0.167 + 0.5z^{-1} - 0.5^{-2} + 0.167z^{-3}. \end{cases} \tag{33}$$
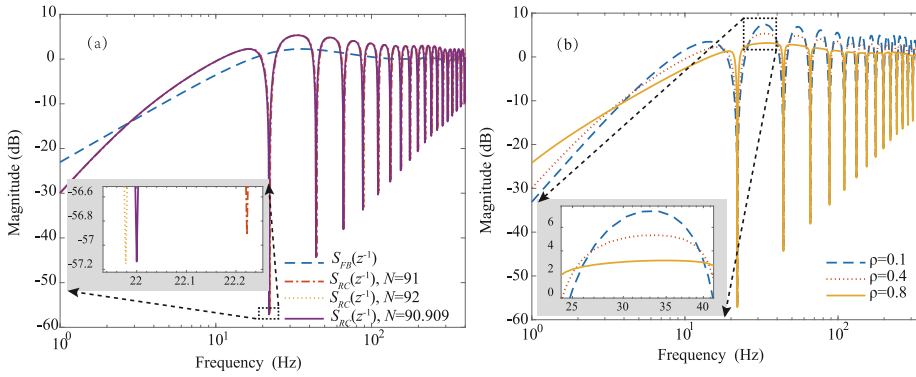
9

Fig. 10. Sensitivity transfer functions of the closed-loop system under different conditions. (a) $S_{FB}(z^{-1})$ and $S_{RC}(z^{-1})$ with $\rho = 0.4$. (b) $S_{RC}(z^{-1})$ with the fractional delay filter for different ρ.
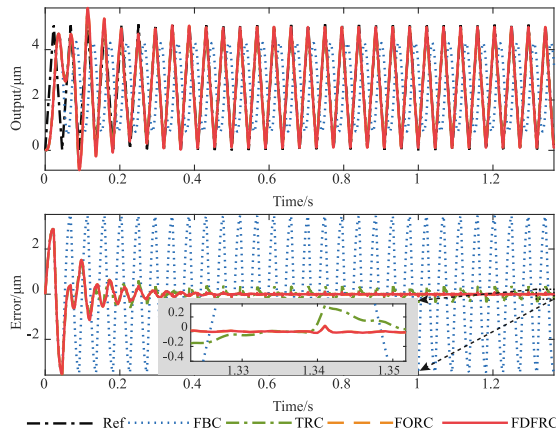

Fig. 11. Tracking performance of different controllers with 22 Hz triangular wave input for x axis.

With $d = 5, \alpha = 0.25, \beta = 0.5$, the sensitivity transfer functions of $S_{FB}(z^{-1})$ and $S_{RC}(z^{-1})$ with different delays under 22 Hz are demonstrated in Fig. 10(a). It can be observed that the proposed FDFRC with fractional delay compensation can generate sufficiently low gains at the foundational frequency and its harmonics of 22 Hz exactly. For $S_{RC}(z^{-1})$ with the integer $N = 91, 92$, the locations of low gains deviate from the desired frequency, which will deteriorate the tracking performance severely. It also should be noted that the implementation of FDFRC will amplify the non-periodic errors shown in Fig. 10(a). Therefore, ρ should be selected appropriately according to the magnitude response of $S_{RC}(z^{-1})$ in Fig. 10(b). The non-periodic errors can be alleviated by a larger ρ. Thus, ρ is set 0.01 in the first 18 periods for fast convergence, and gradually increased to 0.9 in the next periods, then keep it finally to improve robustness in the following experiments.

5. Experimental results

In this section, various experiments are tested to discuss and analyze the proposed method when triangular waves for x axis and Lissajous scanning for $x - y$ axes are as the input references, respectively. Besides the proposed FDFRC, another three controllers are also developed: (1) FBC given in (32); (2) TRC without fractional delay filter [34]; (3) FORC designed by Lagrange interpolation [32].

5.1. Tracking results of triangular waves

In order to test the performance of tracking multi-harmonic reference, the triangular waves commonly used for raster scanning are given as the input for x axis. The frequencies are set as 22 Hz, 24 Hz, and 25 Hz, respectively, and the tracking performance are illustrated in Figs. 11–13. It is evident that the FBC obtains the worst performance at 22 Hz with the root-mean-square error (e_{rms}) and maximum error (e_{max}) at 2.3591 μm and 3.4666 μm, respectively. As we can observe it from Fig. 11, the output amplitude of FBC is much lower than the desired position 5 μm and there exists large phase delay due to the limited closed-loop bandwidth. The similar conclusion can also be obtained through the tracking results shown in Fig. 12 and Fig. 13.

For triangular waves with 22 Hz, the calculated delay parameter N is 90.909, which is non-integer. The experimental results of e_{rms} and e_{max} versus period of 22 Hz reference for different controllers are demonstrated in Fig. 14. The tracking errors of TRC,
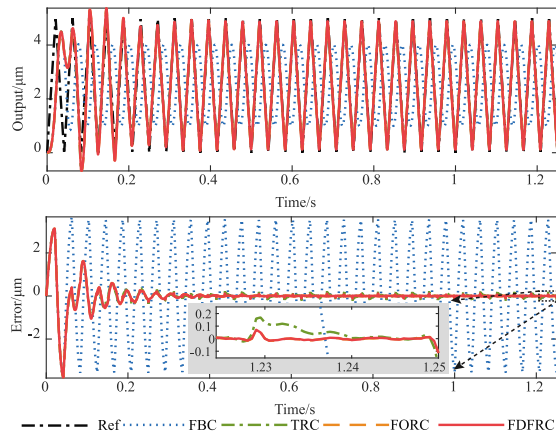
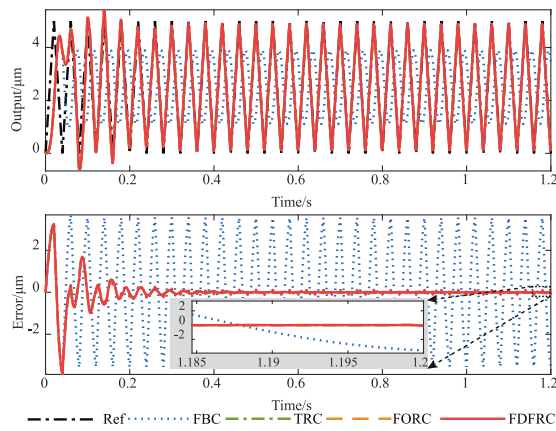**Fig. 12.** Tracking performance of different controllers with 24 Hz triangular wave input for *x* axis.

Fig. 13. Tracking performance of different controllers with 25 Hz triangular wave input for *x* axis.
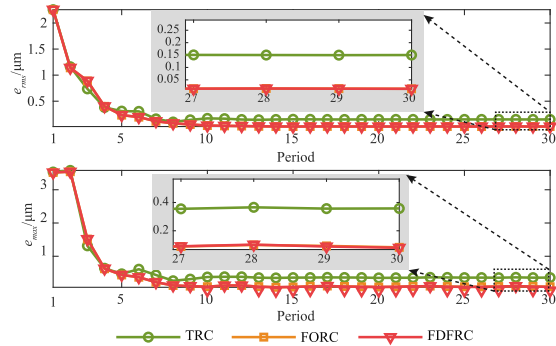

Fig. 14. Experimental results of e_{rms} and e_{max} versus period of 22 Hz reference for different controllers.

FORC, and FDFRC are gradually converged to the steady state with the increasing number of signals' period. Furthermore, the statistical steady-state results in Table 1 are calculated after 20 periods to evaluate the converged performance. The e_{rms} and e_{max} of TRC at 22 Hz is 0.1479 μm and 0.3579 μm, respectively. From the zoom-in figure in Fig. 14, the largest error occurs around the peak of the triangular wave caused by the non-integer delay in TRC. Both FORC and FDFRC could further enhance the tracking performance in comparison with TRC. The e_{rms} and e_{max} are 0.0141 μm and 0.0928 μm for FORC, while 0.0139 μm and 0.0886 μm for FDFRC. The performance of the two controllers is similar because they are all dedicated to deal with the problem of non-integer delay. For the tracking results of 24 Hz with $N = 83.333$, FORC and FDFRC still achieve the best performance at about e_{rms} of

Table 1

Statistical Steady-State Results of Triangular waves for Different Controllers.

Statistical Errors (μm)		22 Hz	24 Hz	25 Hz
FBC	e_{rms}	2.3591	2.3183	2.2907
	e_{max}	3.4666	3.5515	3.5539
TRC	e_{rms}	0.1479	0.0683	0.0222
	e_{max}	0.3579	0.2087	0.1168
FORC	e_{rms}	0.0141	0.0181	0.0223
	e_{max}	0.0928	0.1156	0.1192
FDFRC	e_{rms}	0.0139	0.0181	0.0219
	e_{max}	0.0886	0.1150	0.1178
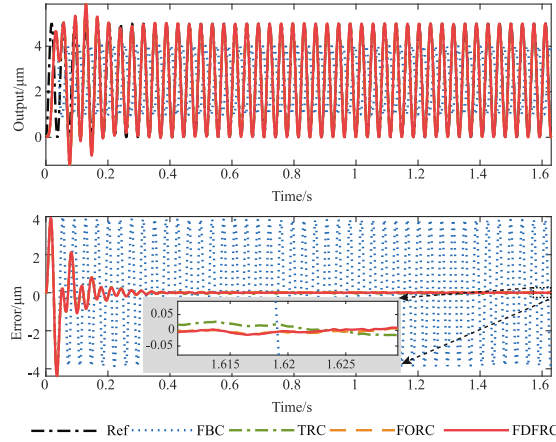
Fig. 15. Tracking performance of different controllers with Lissajous scanning for x axis.

0.0181 μm, e_{max} of 0.1156 μm, i.e, 0.362%, and 2.312% of the tracking stroke, respectively. However, it should be noted that the parameter p determined by the frequency of reference is the only variable in the proposed method because the sub-filters in the Farrow structure are fixed as (33). However, the coefficients using Lagrange interpolating method in FORC should be redesigned for different signals. For example, for the signals' tracking with 22 Hz and 24 Hz, the proposed method only needs to change parameter p from 0.909 to 0.333. In contrast, all the coefficients of integer delay branches in FORC must be calculated off-line and assigned again for implementation. This advantage of FDFRC makes it easy and simple to realize different fractional delays in the fixed sampling rate system.

Furthermore, the 25 Hz reference, i.e. $N = 80$ is fed as the input, and the detailed tracking results are shown in Fig. 13. Due to the integer delay, RC, FORC and FDFRC achieve the similar performance at about e_{rms} of 0.0219 μm, e_{max} of 0.1178 μm, i.e, 0.438%, and 2.356% of the tracking stroke, respectively. The above results demonstrate that the proposed method can improve the tracking performance of triangular waves with various frequencies significantly, and is easier and simpler for practical implementation.

5.2. Tracking results of Lissajous scanning

In the application of scanning imaging in atomic force microscopy, the ratio of x axis and y axis input frequencies for Lissajous scanning should satisfy

$$\frac{f_x}{f_y} = \frac{2M}{2M - 1}, \tag{34}$$

where M is a positive integer. It is clear that it is unavoidable to generate the non-integer delay unless a larger sampling rate is adopted for the control system that may lead to large computing burden. In addition, according to the work in [36], the cross-coupling effects between x and y axis require the sufficient robustness of the controller to external disturbance. Therefore, the tracking results of Lissajous scanning for $x - y$ axes are tested in this subsection, where the references of both axes are sinusoidal waves with 27 Hz and 26.3864 Hz, respectively, which satisfies (34).

The experimental results of x and y axes are plotted in Fig. 15 and Fig. 16, respectively. The tracking results of different controllers in $x–y$ plane are given in Fig. 17. Obviously, the FBC presents the largest tracking errors for the low closed-loop bandwidth so that the scanning area is reduced significantly in comparison with the desired reference as is observed in Fig. 17. The other three controllers are stable even in the present of cross-coupling effects. According to Table 2, the e_{rms} of TRC at steady state are 0.0163 μm and 0.1439 μm for x and y axes, respectively. The proposed method achieves the performance to 0.0055 μm and 0.0088 μm, which improves 66.257% and 94.220%, respectively. Similar to the results of triangular waves, the performance of FORC and FDFRC is
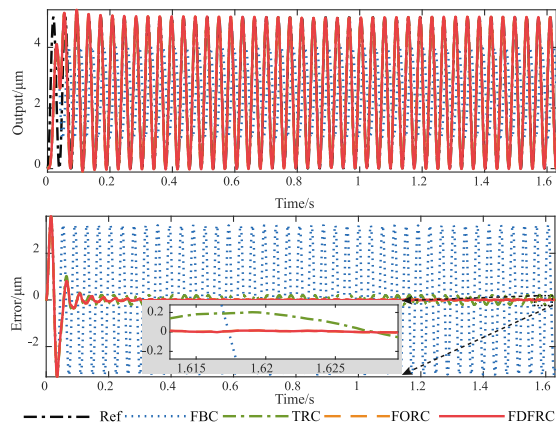
Fig. 16. Tracking performance of different controllers with Lissajous scanning for *y* axis.
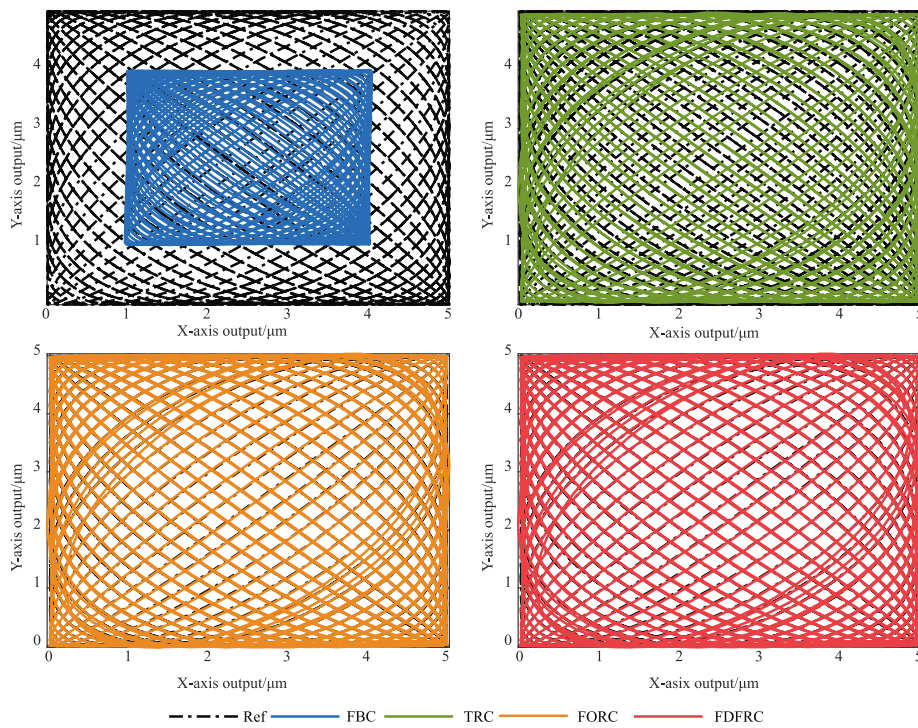

Fig. 17. Tracking performance of different controllers with *x − y* Lissajous scanning.

Table 2
Statistical Steady-State Results of Lissajous Scanning for Different Controllers.

Statistical Errors (μm)		*x* axis	*y* axis
FBC	e_{rms}	2.7213	2.2723
	e_{max}	3.8394	3.2218
TRC	e_{rms}	0.0163	0.1436
	e_{max}	0.0288	0.2061
FORC	e_{rms}	0.0055	0.0083
	e_{max}	0.0131	0.0154
FDFRC	e_{rms}	0.0055	0.0083
	e_{max}	0.0130	0.0158

nearly the same. The detail statistical results are listed in Table 2. However, the proposed method presents the merits of an easy and simple implementation with the only parameter p for x and y axes. The about results demonstrate that the FDFRC can track arbitrary frequencies for Lissajous scanning with high tracking precision.

6. Conclusion

In this paper, a control scheme named FDFRC is proposed for precision tracking of arbitrarily periodic signals. In order to deal with the non-integer delay problem in traditional RC, the fractional delay filter constructed by a Farrow structure is integrated into the spectrum-selection filter so that the infinite gains at the harmonics of the references are achieved even the number of sample points per period of the signal is non-integer. Furthermore, the stability of FDFRC is analyzed in frequency domain to provide the guideline for parameter selection. In comparison with Lagrange interpolation method, the proposed method is with less parameter, easier and simpler to be implemented without redesigned the fractional delay coefficients for different integer/non-integer delays. Moreover, the comparative experiments on a piezoelectric nanopositioning stage are conducted to test the controllers' performance. The results show that the proposed method can improve the tracking performance with various frequencies under integer/non-integer delays significantly for the tracking of triangular waves. The experimental results of $x - y$ Lissajous scanning also verify the high-precision performance of the proposed method comparing with the other controllers.

Although the proposed method can track arbitrarily periodic signals, the implementation of the spectrum-selection filter will always amplify the non-periodic errors to a certain extent. In the further work, the feedback controller like sliding mode control [43] or observer technology [18,19] will be explored to enhance the robustness of the overall system.

CRediT authorship contribution statement

Zhao Feng: Methodology, Validation, Data curation, Writing – original draft. **Min Ming:** Validation. **Jie Ling:** Writing – review & editing. **Xiaohui Xiao:** Funding acquisition. **Zhi-Xin Yang:** Funding acquisition. **Feng Wan:** Funding acquisition.

Declaration of competing interest

The authors declare that they have no known competing financial interests or personal relationships that could have appeared to influence the work reported in this paper.

Acknowledgments

References

[1] Z. Zhang, X. Wang, J. Liu, C. Dai, Y. Sun, Robotic micromanipulation: Fundamentals and applications, Annu. Rev. Control Robot. Auton. Syst. 2 (2019) 181–203.
[2] L. Wang, W. Chen, J. Liu, J. Deng, Y. Liu, A review of recent studies on non-resonant piezoelectric actuators, Mech. Syst. Signal Process. 133 (2019) 106254.
[3] M. Ling, L.L. Howell, J. Cao, G. Chen, Kinetostatic and dynamic modeling of flexure-based compliant mechanisms: a survey, Appl. Mech. Rev. 72 (3).
[4] Y. Wei, Q. Xu, A survey of force-assisted robotic cell microinjection technologies, IEEE Trans. Autom. Sci. Eng. 16 (2) (2018) 931–945.
[5] Z. Zhu, H. Du, R. Zhou, P. Huang, W.-L. Zhu, P. Guo, Design and trajectory tracking of a nanometric ultra-fast tool servo, IEEE Trans. Ind. Electron. 67 (1) (2019) 432–441.
[6] S.K. Das, F.R. Badal, M.A. Rahman, M.A. Islam, S.K. Sarker, N. Paul, Improvement of alternative non-raster scanning methods for high speed atomic force microscopy: A review, IEEE Access 7 (2019) 115603–115624.
[7] D. Sabarianand, P. Karthikeyan, T. Muthuramalingam, A review on control strategies for compensation of hysteresis and creep on piezoelectric actuators based micro systems, Mech. Syst. Signal Process. 140 (2020) 106634.
[8] G.-Y. Gu, L.-M. Zhu, C.-Y. Su, H. Ding, S. Fatikow, Modeling and control of piezo-actuated nanopositioning stages: A survey, IEEE Trans. Autom. Sci. Eng. 13 (1) (2014) 313–332.
[9] Z. Feng, W. Liang, J. Ling, X. Xiao, K.K. Tan, T.H. Lee, Integral terminal sliding-mode-based adaptive integral backstepping control for precision motion of a piezoelectric ultrasonic motor, Mech. Syst. Signal Process. 144 (2020) 106856.
[10] J. Ling, M. Rakotondrabe, Z. Feng, M. Ming, X. Xiao, A robust resonant controller for high-speed scanning of nanopositioners: design and implementation, IEEE Trans. Control Syst. Technol. 28 (3) (2019) 1116–1123.
[11] B.A. Francis, W.M. Wonham, The internal model principle of control theory, Automatica 12 (5) (1976) 457–465.
[12] Z. Feng, J. Ling, M. Ming, X. Xiao, Integrated modified repetitive control with disturbance observer of piezoelectric nanopositioning stages for high-speed and precision motion, J. Dyn. Syst. Measur. Control 141 (8).
[13] Z. Feng, J. Ling, M. Ming, X. Xiao, A model-data integrated iterative learning controller for flexible tracking with application to a piezo nanopositioner, Trans. Inst. Meas. Control 40 (10) (2018) 3201–3210.
[14] C.T. Freeman, M.A. Alsubaie, Z. Cai, E. Rogers, P.L. Lewin, A common setting for the design of iterative learning and repetitive controllers with experimental verification, Internat. J. Adapt. Control Signal Process. 27 (3) (2013) 230–249.

[15] L. Wang, C.T. Freeman, E. Rogers, D.H. Owens, Experimentally validated continuous-time repetitive control of non-minimum phase plants with a prescribed degree of stability, Control Eng. Pract. 18 (10) (2010) 1158–1165.

[16] P. Dabkowski, K. Galkowski, O. Bachelier, E. Rogers, M. Sebek, A. Kummert, Control of differential linear repetitive processes using strong practical stability and h-inf disturbance attenuation, Internat. J. Control 86 (4) (2013) 636–649.

[17] L. Wang, C.T. Freeman, S. Chai, E. Rogers, Predictive-repetitive control with constraints: From design to implementation, J. Process Control 23 (7) (2013) 956–967.

[18] R. Sakthivel, S. Mohanapriya, H.R. Karimi, P. Selvaraj, A robust repetitive-control design for a class of uncertain stochastic dynamical systems, IEEE Trans. Circuits Syst. II Express Briefs 64 (4) (2016) 427–431.

[19] R. Sakthivel, L. Susana Ramya, P. Selvaraj, Observer-based state tracking control of uncertain stochastic systems via repetitive controller, Internat. J. Systems Sci. 48 (11) (2017) 2272–2281.

[20] Y. Shan, K.K. Leang, Accounting for hysteresis in repetitive control design: Nanopositioning example, Automatica 48 (8) (2012) 1751–1758.

[21] Y. Shan, K.K. Leang, Design and control for high-speed nanopositioning: serial-kinematic nanopositioners and repetitive control for nanofabrication, IEEE Control Syst. Mag. 33 (6) (2013) 86–105.

[22] C.-X. Li, G.-Y. Gu, L.-M. Zhu, C.-Y. Su, Odd-harmonic repetitive control for high-speed raster scanning of piezo-actuated nanopositioning stages with hysteresis nonlinearity, Sensors Actuators A 244 (2016) 95–105.

[23] Y.R. Teo, Y. Yong, A.J. Fleming, A comparison of scanning methods and the vertical control implications for scanning probe microscopy, Asian J. Control 20 (4) (2018) 1352–1366.

[24] Z. Liu, B. Zhang, K. Zhou, Universal fractional-order design of linear phase lead compensation multirate repetitive control for PWM inverters, IEEE Trans. Ind. Electron. 64 (9) (2017) 7132–7140.

[25] D. Wang, X. Chen, A multirate fractional-order repetitive control for laser-based additive manufacturing, Control Eng. Pract. 77 (2018) 41–51.

[26] F. Padula, A. Visioli, Tuning rules for optimal PID and fractional-order PID controllers, J. Process Control 21 (1) (2011) 69–81.

[27] R. De Keyser, C.I. Muresan, C.M. Ionescu, A novel auto-tuning method for fractional order PI/PD controllers, ISA Trans. 62 (2016) 268–275.

[28] R. De Keyser, C.I. Muresan, C.M. Ionescu, An efficient algorithm for low-order direct discrete-time implementation of fractional order transfer functions, ISA Trans. 74 (2018) 229–238.

[29] C. Ding, J. Cao, Y. Chen, Fractional-order model and experimental verification for broadband hysteresis in piezoelectric actuators, Nonlinear Dynam. 98 (4) (2019) 3143–3153.

[30] Y. Chen, I. Petras, D. Xue, Fractional order control-a tutorial, in: 2009 American Control Conference, IEEE, 2009, pp. 1397–1411.

[31] C.M. Ionescu, E.H. Dulf, M. Ghita, C.I. Muresan, Robust controller design: Recent emerging concepts for control of mechatronic systems, J. Franklin Inst. B 357 (12) (2020) 7818–7844.

[32] Q. Zhao, Y. Ye, Fractional phase lead compensation RC for an inverter: Analysis, design, and verification, IEEE Trans. Ind. Electron. 64 (4) (2016) 3127–3136.

[33] L. Li, G. Gu, L. Zhu, Fractional repetitive control of nanopositioning stages for tracking high-frequency periodic inputs with nonsynchronized sampling, Rev. Sci. Instrum. 90 (5) (2019) 055108.

[34] X. Chen, M. Tomizuka, New repetitive control with improved steady-state performance and accelerated transient, IEEE Trans. Control Syst. Technol. 22 (2) (2013) 664–675.

[35] L. Li, S.S. Aphale, L. Zhu, Enhanced odd-harmonic repetitive control of nanopositioning stages using spectrum-selection filtering scheme for high-speed raster scanning, IEEE Trans. Autom. Sci. Eng.

[36] Z. Feng, J. Ling, M. Ming, W. Liang, K.K. Tan, X. Xiao, Signal-transformation-based repetitive control of spiral trajectory for piezoelectric nanopositioning stages, IEEE/ASME Trans. Mechatronics 25 (3) (2020) 1634–1645.

[37] L. Dai, X. Li, Y. Zhu, M. Zhang, Quantitative tracking error analysis and feedforward compensation under different model-based feedforward controllers in different control architectures, IEEE Trans. Ind. Electron. 68 (1) (2020) 381–390.

[38] M. Rivero, S.V. Rogosin, J.A. Tenreiro Machado, J.J. Trujillo, Stability of fractional order systems, Math. Probl. Eng. (2013).

[39] R. Nazir, K. Zhou, N. Watson, A. Wood, Analysis and synthesis of fractional order repetitive control for power converters, Electr. Power Syst. Res. 124 (2015) 110–119.

[40] J. Na, R. Costa-Castelló, R. Grino, X. Ren, Discrete-time repetitive controller for time-delay systems with disturbance observer, Asian J. Control 14 (5) (2012) 1340–1354.

[41] T. Liu, D. Wang, K. Zhou, High-performance grid simulator using parallel structure fractional repetitive control, IEEE Trans. Power Electron. 31 (3) (2015) 2669–2679.

[42] C.-X. Li, G.-Y. Gu, M.-J. Yang, L.-M. Zhu, High-speed tracking of a nanopositioning stage using modified repetitive control, IEEE Trans. Autom. Sci. Eng. 14 (3) (2015) 1467–1477.

[43] S. Gambhire, D.R. Kishore, P. Londhe, S. Pawar, Review of sliding mode based control techniques for control system applications, Int. J. Dyn. Control 9 (2021) 363–378.